Supplementary Information

Orthogonalization of spontaneous and stimulus-driven activity by hierarchical neocortical areal network in primates

Teppei Matsui*, Takayuki Hashimoto*, Tomonari Murakami, Masato Uemura, Kohei Kikuta, Toshiki Kato, Kenichi Ohki*

Correspondence to Kenichi Ohki (kohki@m.u-tokyo.ac.jp), Teppei Matsui (tematsui@mail.doshisha.ac.jp), and Takayuki Hashimoto (hashimoto@m.u-tokyo.ac.jp)

This PDF file includes:

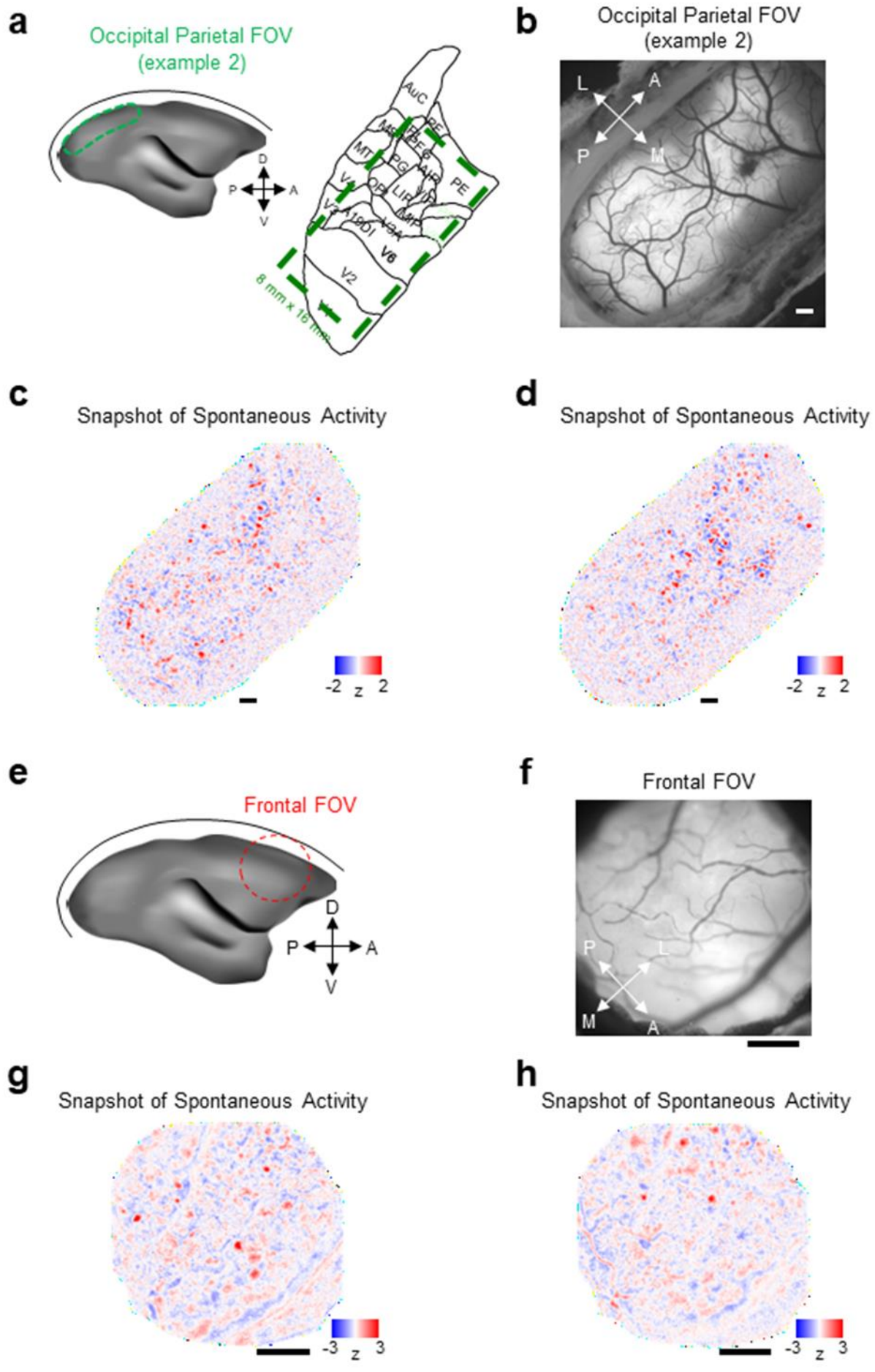
a
Occipital Parietal FOV
(example 2)
D
P
A
V
AuC
PE
MST
FEF
MT
PG
AIP
V4
OP
LIP
PE
V3A
19d
MIP
V3A
V6
V2
8 mm x 16 mm
b
Occipital Parietal FOV
(example 2)
L
A
P
M
c
Snapshot of Spontaneous Activity
-2
z
2
d
Snapshot of Spontaneous Activity
-2
z
2
e
Frontal FOV
D
P
A
V
f
Frontal FOV
P
L
M
A
g
Snapshot of Spontaneous Activity
-3
z
3
h
Snapshot of Spontaneous Activity
-3
z
3

Supplementary Figure 1 | Examples of patchy spontaneous activity in the parietal and frontal areas. **(a-d)** Spontaneous activity in the FOV including the parietal areas. **(a)** The approximate position of the FOV on the marmoset brain atlas (75). This chapter was published in Elsevier Science, G. Paxinos, C. Watson, M. Petrides, M. Rosa, H. Tokuno, The Marmoset Brain in Stereotaxic Coordinates, pp. 324, Copyright Elsevier Science (2011). **(b)** FOV image showing in vivo GCaMP fluorescence. **(c)-(d)** Snapshots of spontaneous activities. **(e-h)** Snapshots of spontaneous activity in FOV including the frontal areas. (b) Approximate position of FOV. Same convention as Fig. 1a (b) FOV image showing in vivo GCaMP fluorescence. (c)-(d) Snapshots of spontaneous activity. Scale bars, 1 mm.

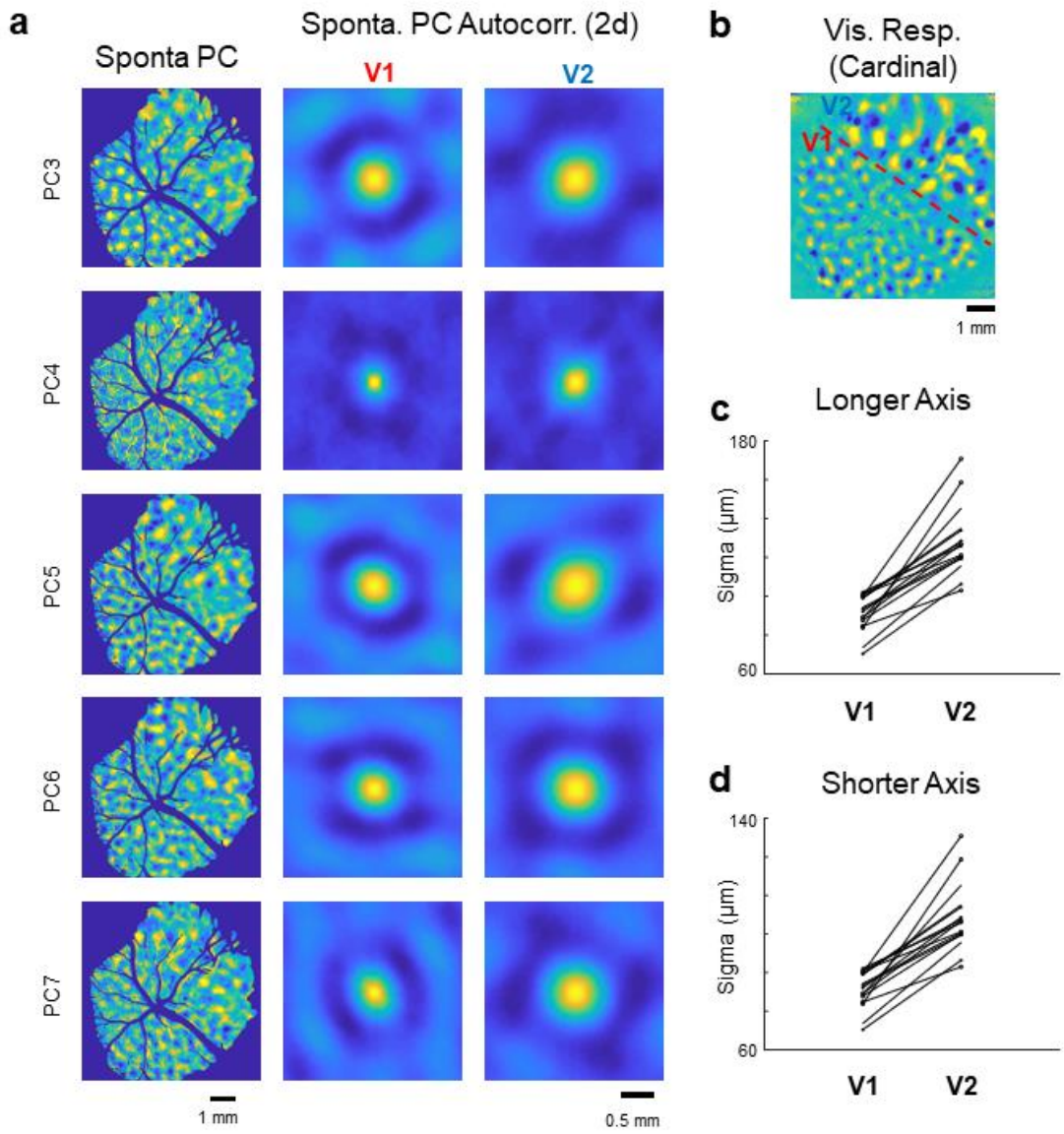

Supplementary Figure 2 | Size of spontaneous patches varied across cortical areas. (a) Left column, principal components (PCs) of spontaneous activity for a FOV covering V1 and V2. PC#3-7 are shown. PC#1 and PC#2 are discarded because these PCs mainly reflected vascular noise (see also Supplementary Fig. 13). Middle and right columns, spatial autocorrelation maps of PCs obtained using pixels in V1 (middle) and V2 (right). For all PCs, autocorrelation peaks in V2 were broader than those in V1. **(b)** A visually evoked orientation response in the same FOV as (a). **(c-d)** Quantification of the sizes of the autocorrelation peaks in V1 and V2. Data from three FOVs covering V1 and V2 were used [including a FOV shown in (a)]. Five PCs are obtained from each FOV. For each PC, autocorrelation peaks in V1 and V2 are fitted with two-dimensional Gaussians. Lines in (c) and (d) connects datapoints taken from the same PC in the same FOV. Autocorrelation peaks are larger in V2 than in V1 for both longer (c) and shorter axes (d) (mean difference, 19.9%). Note that we did not perform statistical testing for (c) and (d) because data points are not statistically independent (5 PCs were obtained from each of FOV).

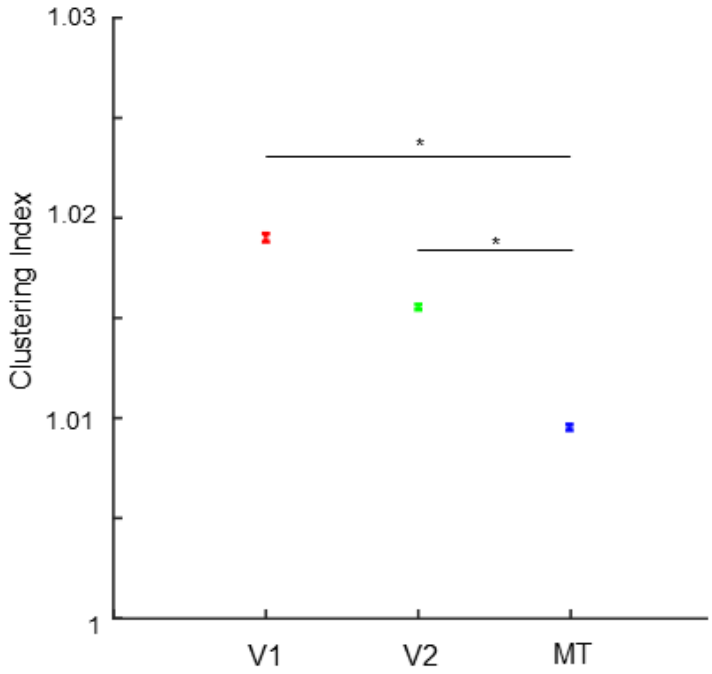

Supplementary Figure 3 | Clustering of cellular spontaneous activity differs across areas. For each spontaneous frame, the degree of clustering of spatial clustering of active neurons is assessed (see Methods). A larger clustering index indicates more spatial clustering of active neurons. The degree of clustering decreased in higher visual areas (*, $p < 0.001$, Kolmogorov-Smirnov test, corrected by Bonferroni's method; **, $P = 0.0481$, Kolmogorov-Smirnov test, uncorrected). Error bar, SEM.

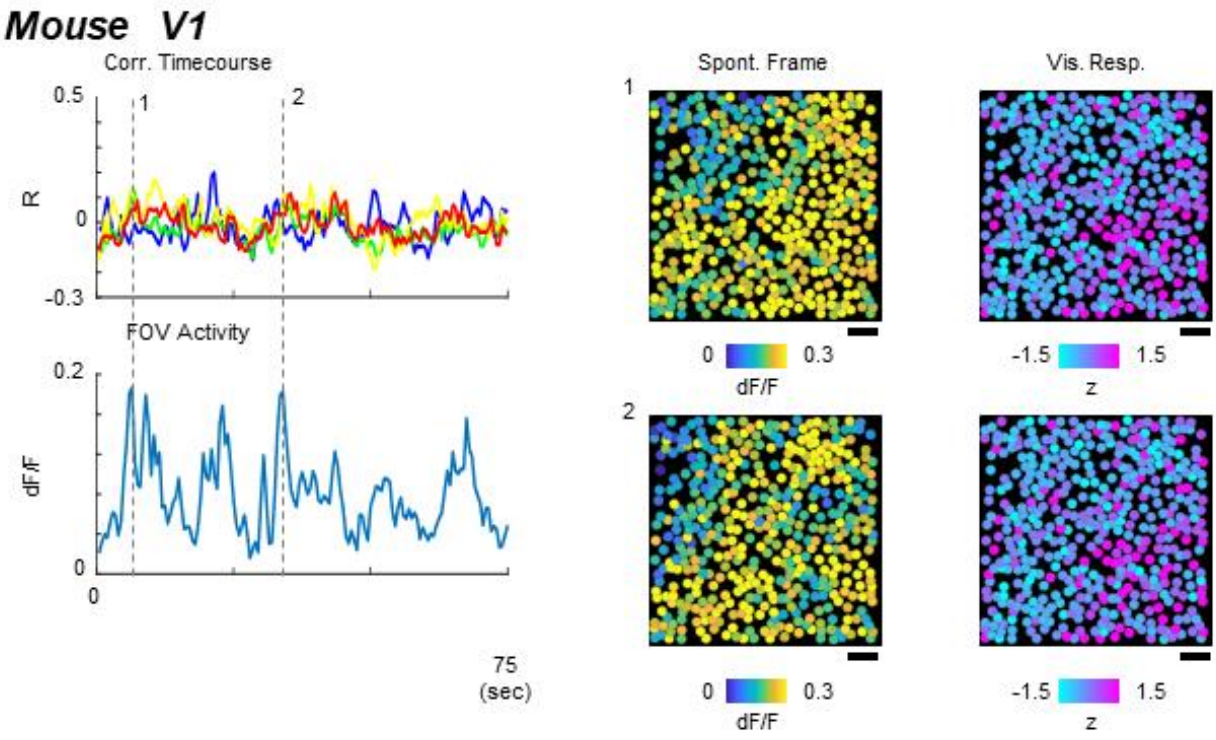

Supplementary Figure 4 | Example cellular spontaneous and evoked activity in mouse V1. Same convention as in Fig. 2d-f but for an example FOV in mouse V1 (b). Scale bars, 100 μm.

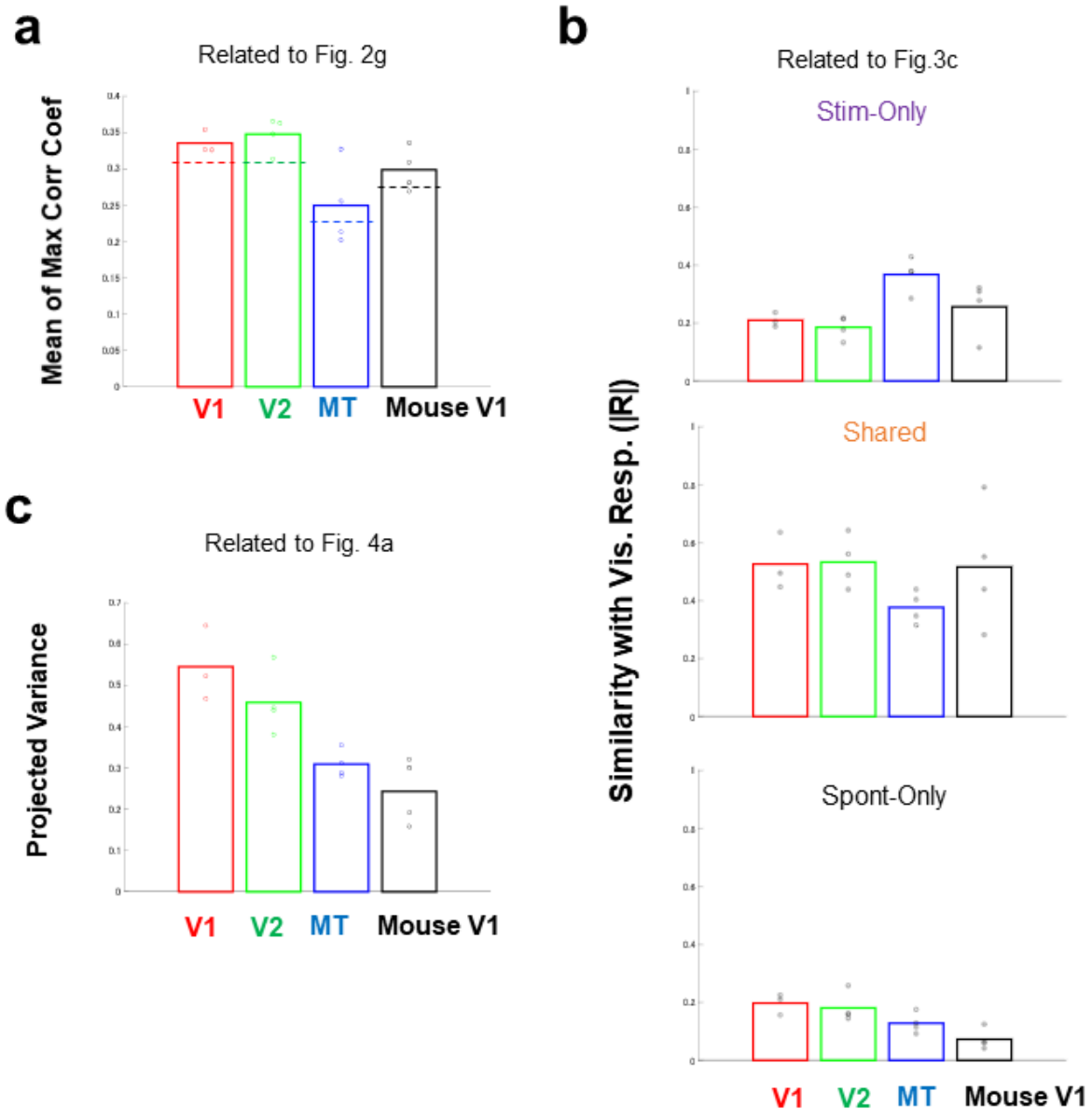

Supplementary Figure 5 | Results summarized by animals. a) Max Correlation Coefficients (same as in Fig. 2g) across visual areas. Mean values across animals are shown. The dotted line indicates median values across all concatenated spontaneous frames (the distribution shown in Fig. 2g). **b**) Same as Fig. 3c but data are summarized by animals. **c**) Same as Fig. 4a but data are summarized by animals.

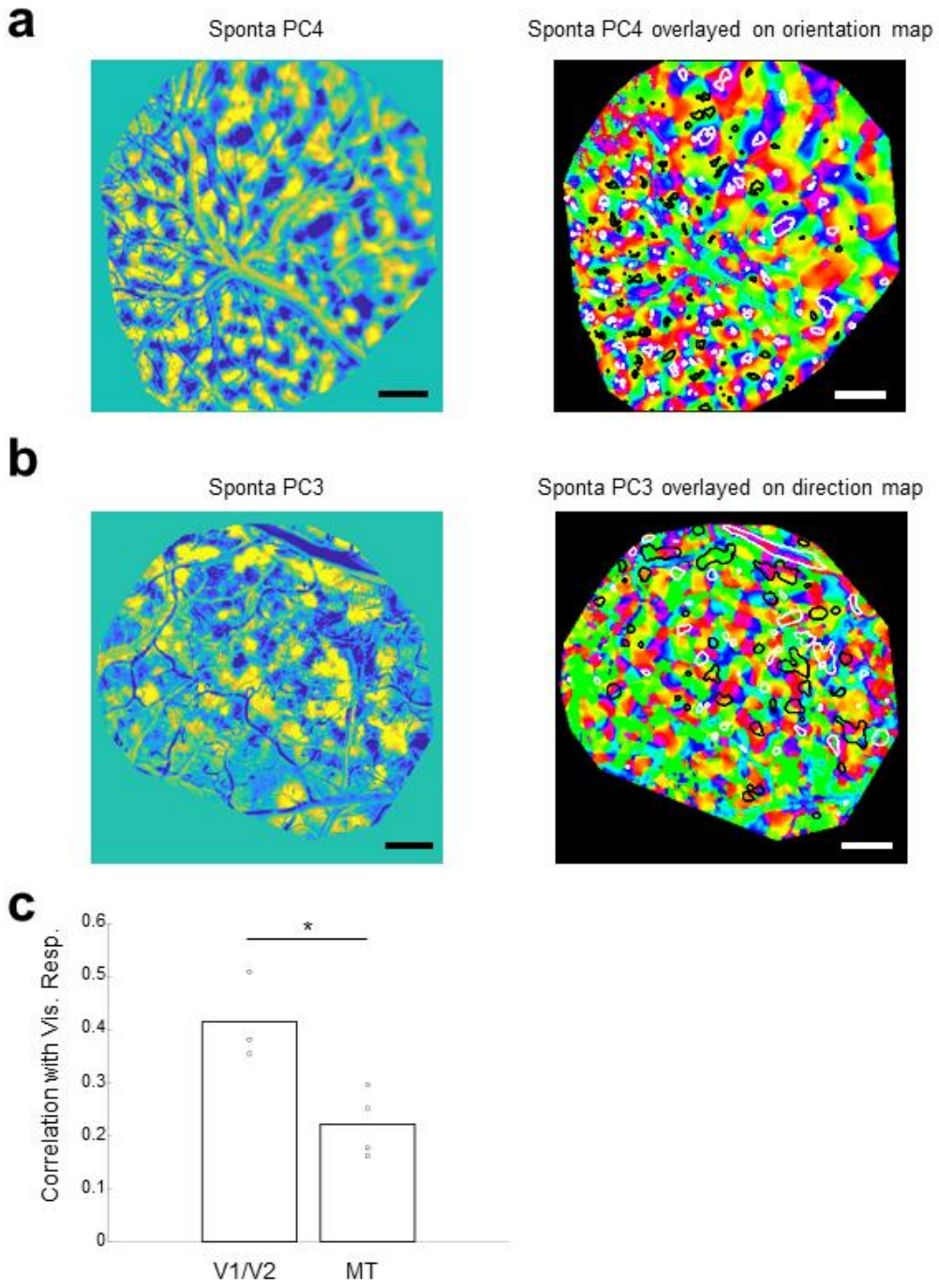

Supplementary Figure 6 | Comparisons of spontaneous PCs and visually evoked maps. a) An example of a FOV in V1/V2. Left, an example of spontaneous PC that resembled an orientation-evoked response. Right, a map of preferred orientations. White and black contours indicate locations of the positive (yellow) peaks and negative (blue) peaks in the spontaneous PC, respectively. **b**) Same convention as (a) but for an example FOV in MT. Left, spontaneous PC. Right, a map of preferred directions. **c)** Spatial correlation between spontaneous PCs and orientation/direction maps. For each FOV, the highest correlation between orientation (V1/V2) or direction (MT) evoked response was calculated. The spatial correlation between spontaneous PCs and functional maps was significantly higher in V1/V2 than in MT ($p < 0.017$, two-sample t test). Scale bars, 1 mm.

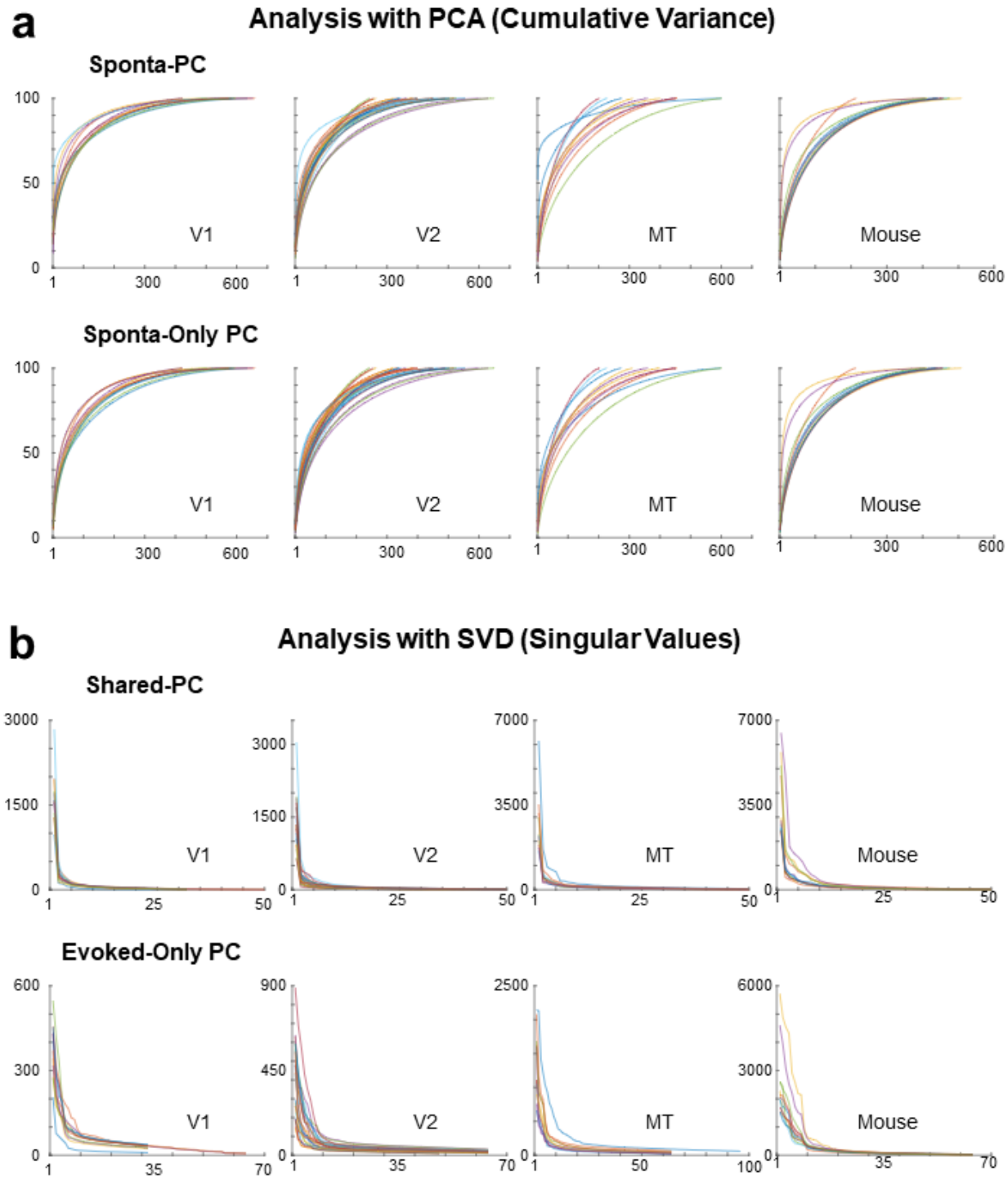

Supplementary Figure 7 | Data related to PCA and SVD of cellular scale neural activity. a) Plots of cumulative explained variance for PCAs which are used to obtain spontaneous PCs (top) and spontaneous-only PCs (bottom). Each trace indicates the cumulative explained variance for one FOV. **b**) Plots of singular values for SVDs which are used to obtain shared PCs (top) and evoked-only PCs (bottom). Each trace indicates the plot of singular values for one FOV.

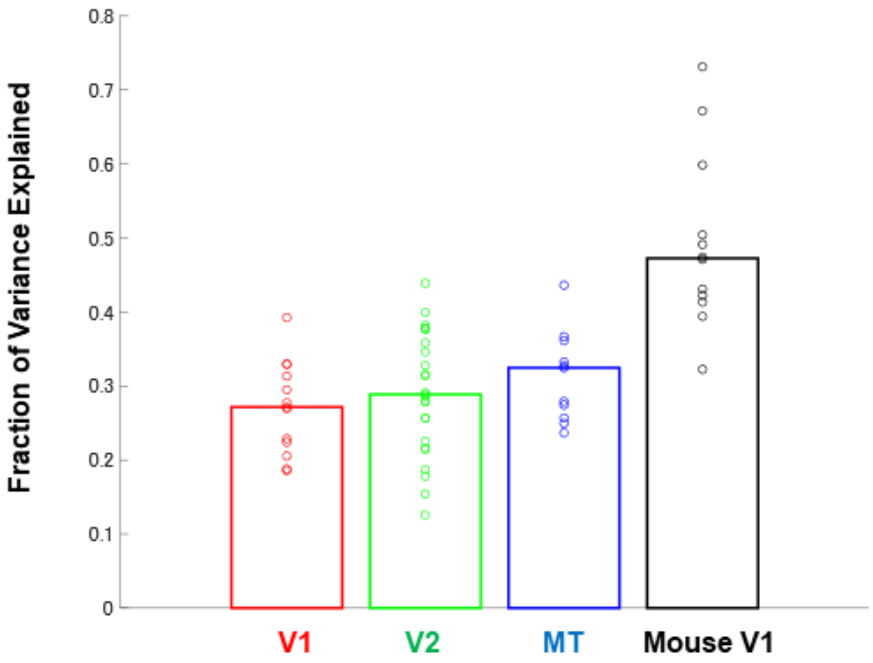

Supplementary Figure 8 | Fractions of the variance of single-trial stimulus-evoked activity explained by trial-averaged stimulus-evoked activity.

Fractions of the variance of single-trial stimulus-evoked activity explained by trial-averaged stimulus-evoked activity as estimated by cross-validated regression. For the cross-validated regression, trials are split into halves. One half was used to obtain trial-averaged activity, and the other half is used to estimate the variance.

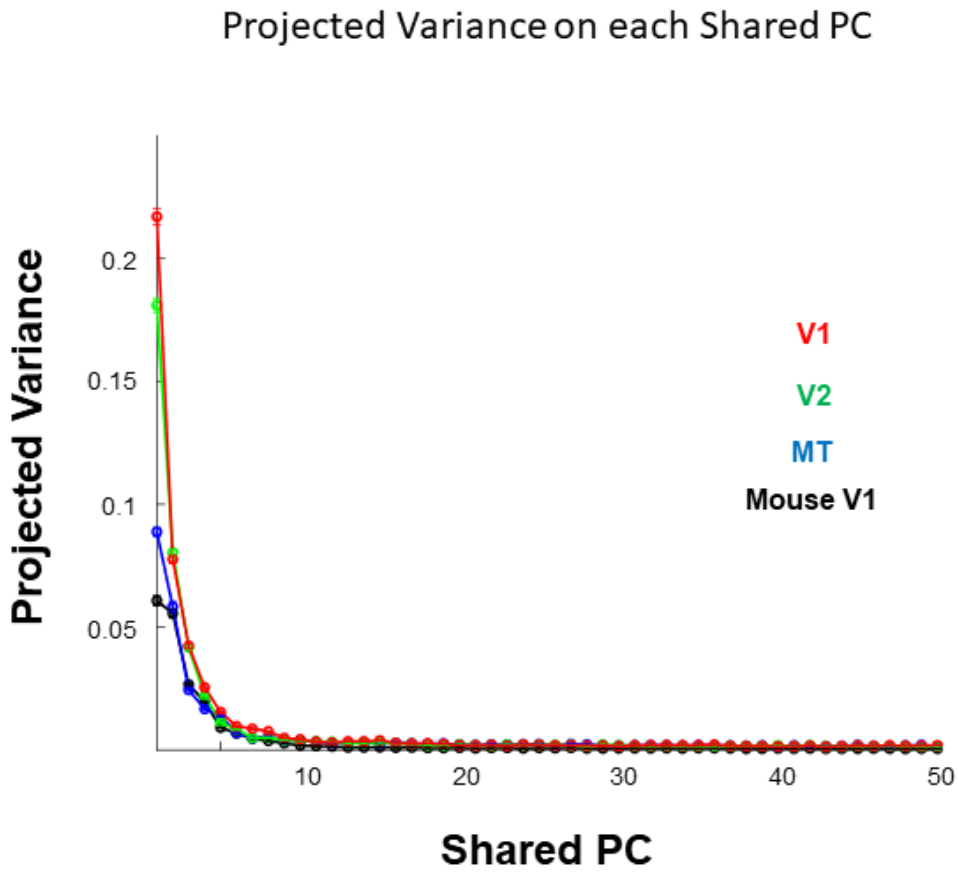

Supplementary Figure 9 | Stimulus-related variance projected onto each shared PC. The variance of cellular-level trial-averaged visual responses projected to individual PCs of the Shared subspace. Same as Figure 4b but a projection to 50 Shared PCs is shown.

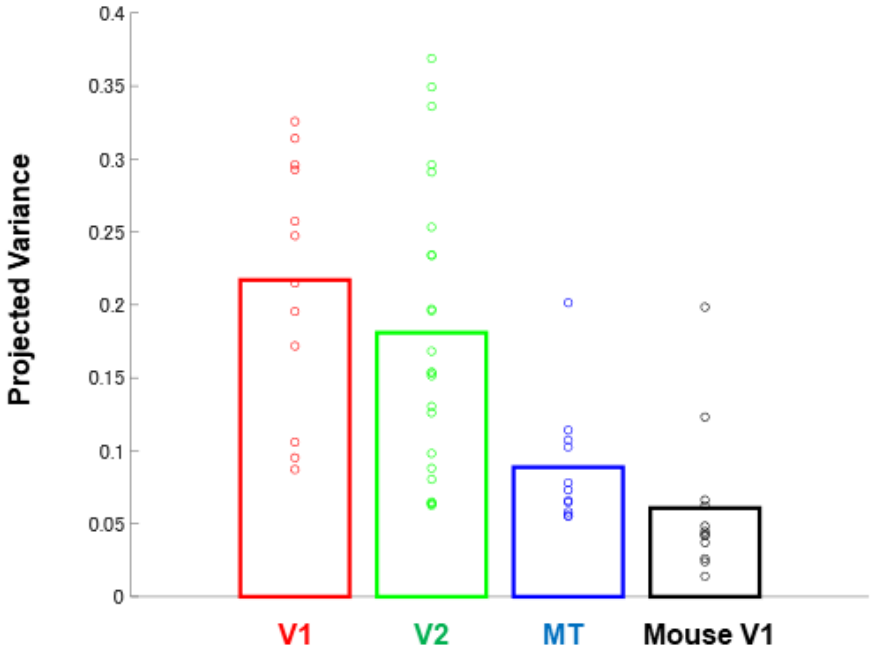

Supplementary Figure 10 | Stimulus-related variance projected onto one-dimensional shared space.

Same convention as Figure 4a but projected variances were calculated using only the 1st shared PCs.

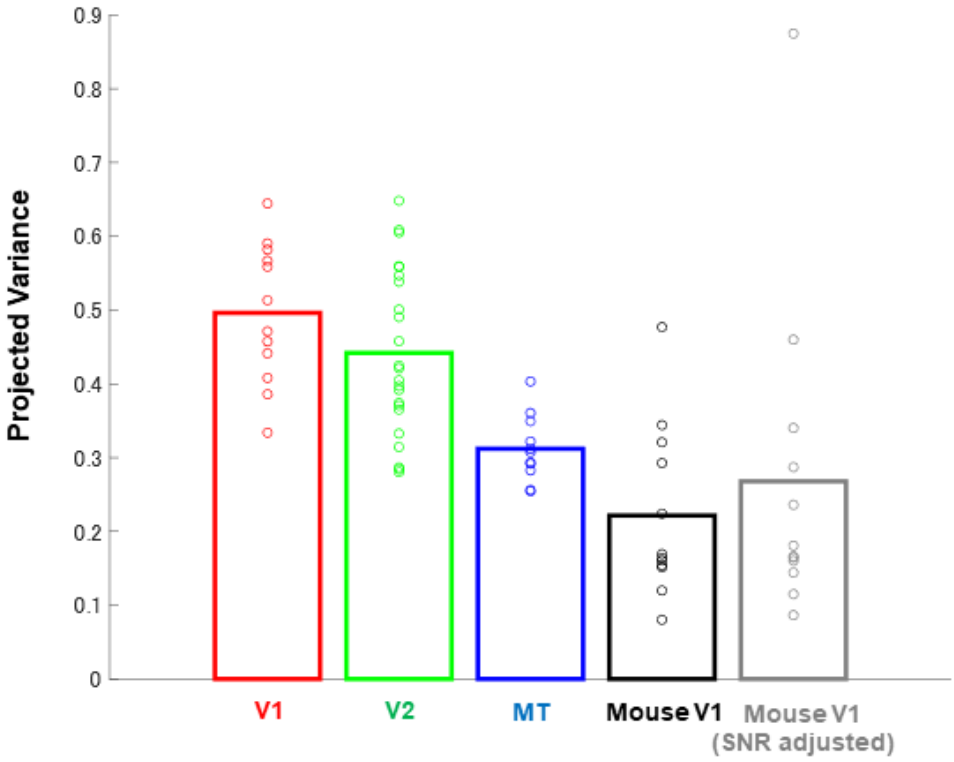

Supplementary Figure 11 | Stimulus-related variance projected onto shared space with SNR adjusted estimate of the mouse V1. Variance in cellular-level trial-averaged visual responses projected onto the shared subspace. V1, V2, MT, and Mouse V1 show the same data as in Fig. 4a. "Mouse V1 (SNR adjusted)" (gray)indicates the projected variance after the correction for potential SNR difference between mouse and marmoset imaging. Because of the difference in FOV size, the number of pixels allocated to one neuron is larger for the mouse than for the marmosets, which could yield a better SNR for the mouse. To rule out the possibility that this difference affected the overall results, we re-analysed the mouse data, with the number of pixels allocated to each cell being comparable to that of the marmoset. The median numbers of pixels allocated to each cell in the marmoset and mouse V1 are 110 and 208, respectively. To match the number of pixels allocated to each cell in mouse V1, we randomly selected 100 pixels within the original cell-mask and used them to obtain new cell time courses. These new cell time courses are then used to calculate the stimulus-related variance projected onto a shared space. The overall results of this control analysis do not differ from the original results; the value of the projected variance obtained with the new time courses of the mouse V1 is smaller than that of the marmoset visual cortex. Moreover, the projected variance of the mouse V1 calculated using the new and original time courses do not show a statistically significant difference ($p > 0.1$, Wilcoxon signed-rank test).

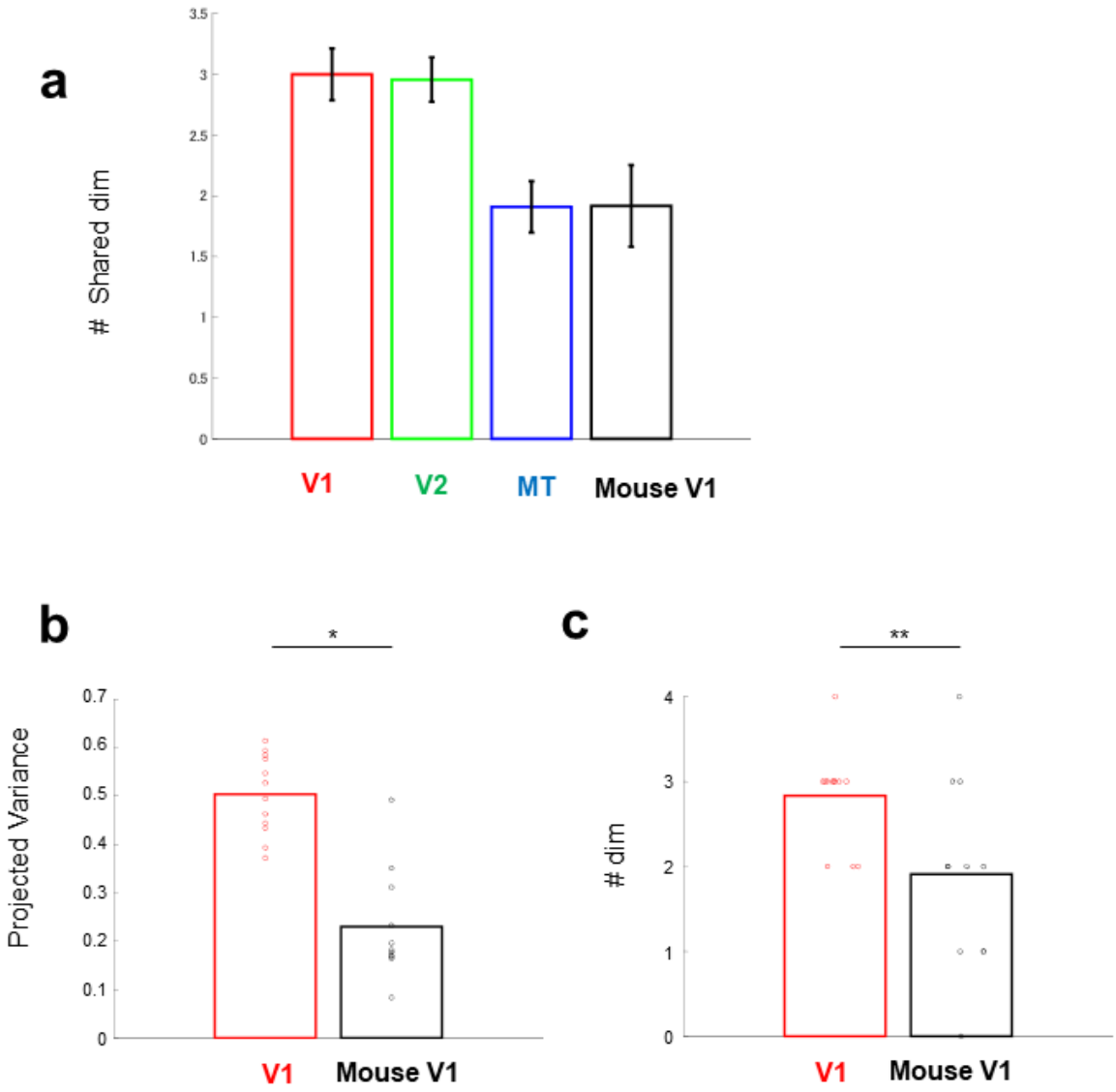

Supplementary Figure 12 | Estimated numbers of dimension of shared space and control analysis with a fixed number of trials and cells. a) Numbers of dimensions of shared space across visual areas. The mean number of remaining PCs and the amount of projected variance explained by the remaining components are as follows: V1: 3.0, 34.1%; V2 3.0, 30.8%; MT, 1.9, 14.6%; Mouse V1: 1.9, 12.1% [Area Name: mean number of remaining shared PCs, mean of total explained variance projected onto the remaining components]. Regarding the use of 50 PCs in the initial step, we agree with the reviewer that the choice of 50 PCs in the initial step could have affected these results. **b-c**) Control analysis conducted with a fixed number of trials (20) and cells (400). (b) shows fractions of stimulus-related variance projected onto shared spaces in marmoset V1 and mouse V1. The amount of the projected variance is significantly larger in marmoset V1 than in mouse V1 ($p < 0.00001$, two-sample *t*-test). (c) Estimated numbers of dimensions of shared space in marmoset V1 and mouse V1. The estimated numbers of dimensions are significantly larger in marmoset V1 than in mouse V1 ($p< 0.03$, two-sample *t*-test).

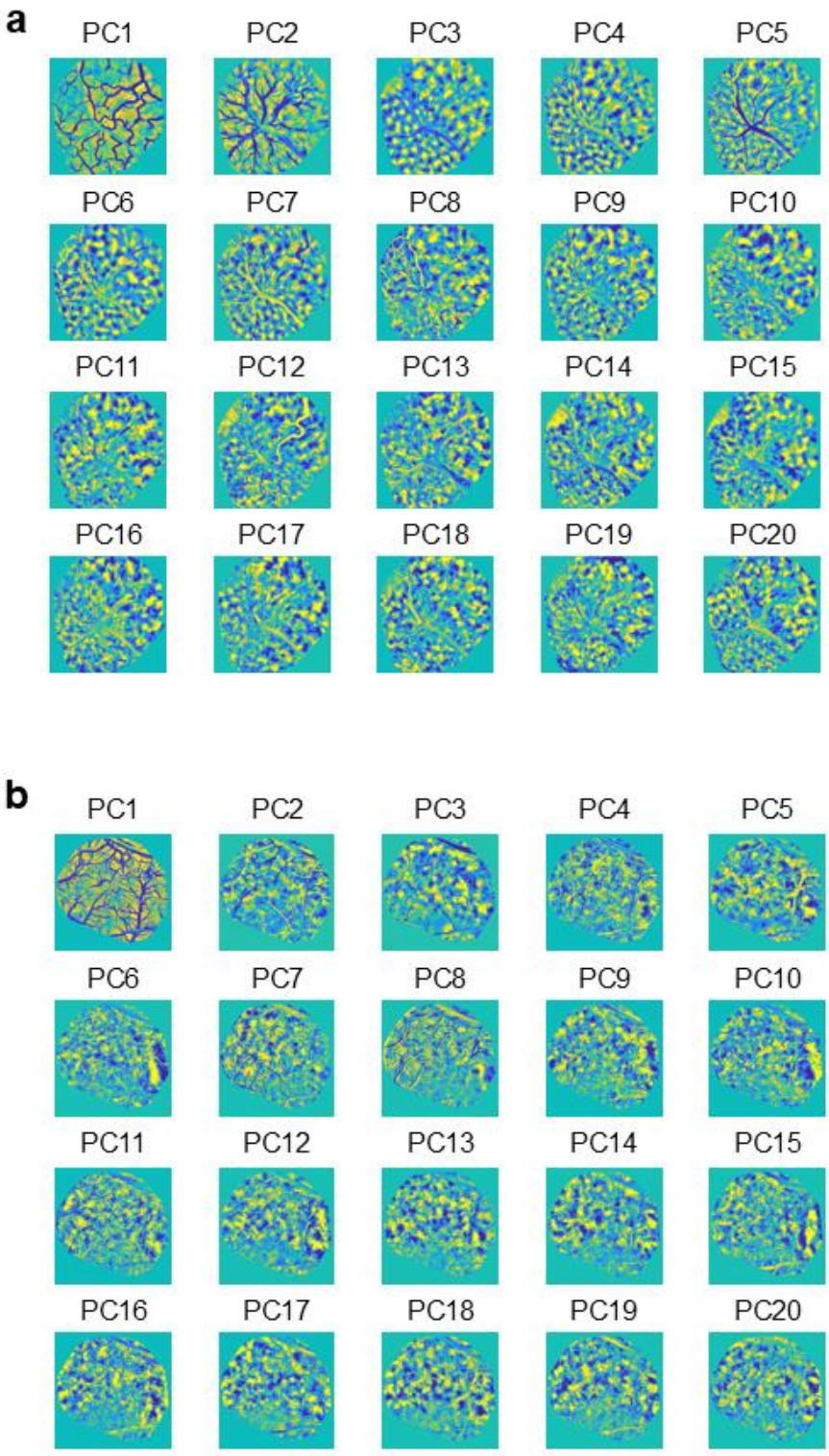

Supplementary Figure 13 | Examples of spontaneous PCs in widefield imaging. The top 20 PCs of spontaneous activity are shown for two example FOVs. **a**) V1/V2 FOV. **b**) MT FOV.

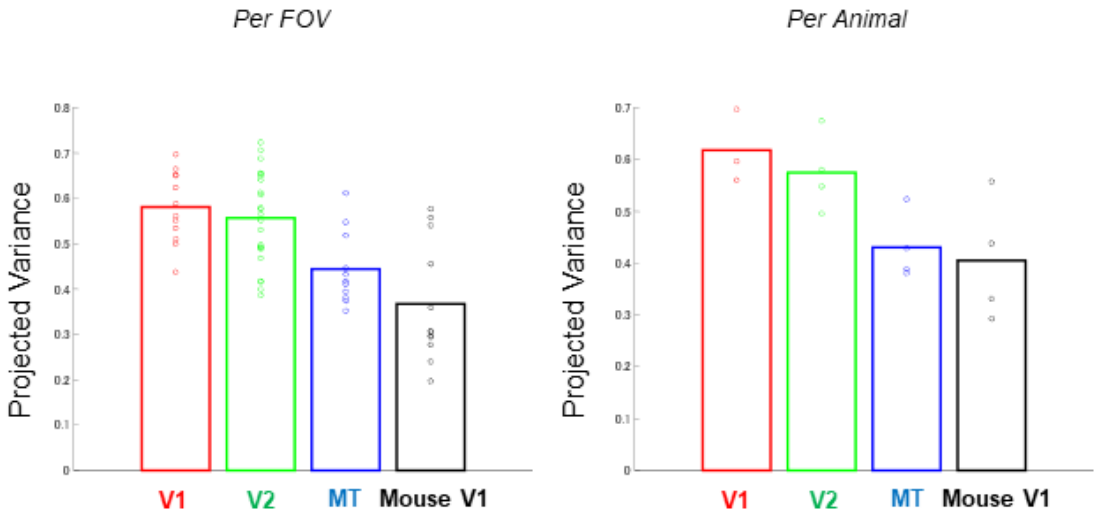

Supplementary Figure 14 | Stimulus-related variance projected onto 100-dimensional shared space. Left, same convention as Figure 4a but projected variances are calculated using 100-dimensional shared space. Each point indicates FOV. Right, same as the left but the data are summarized by animals.

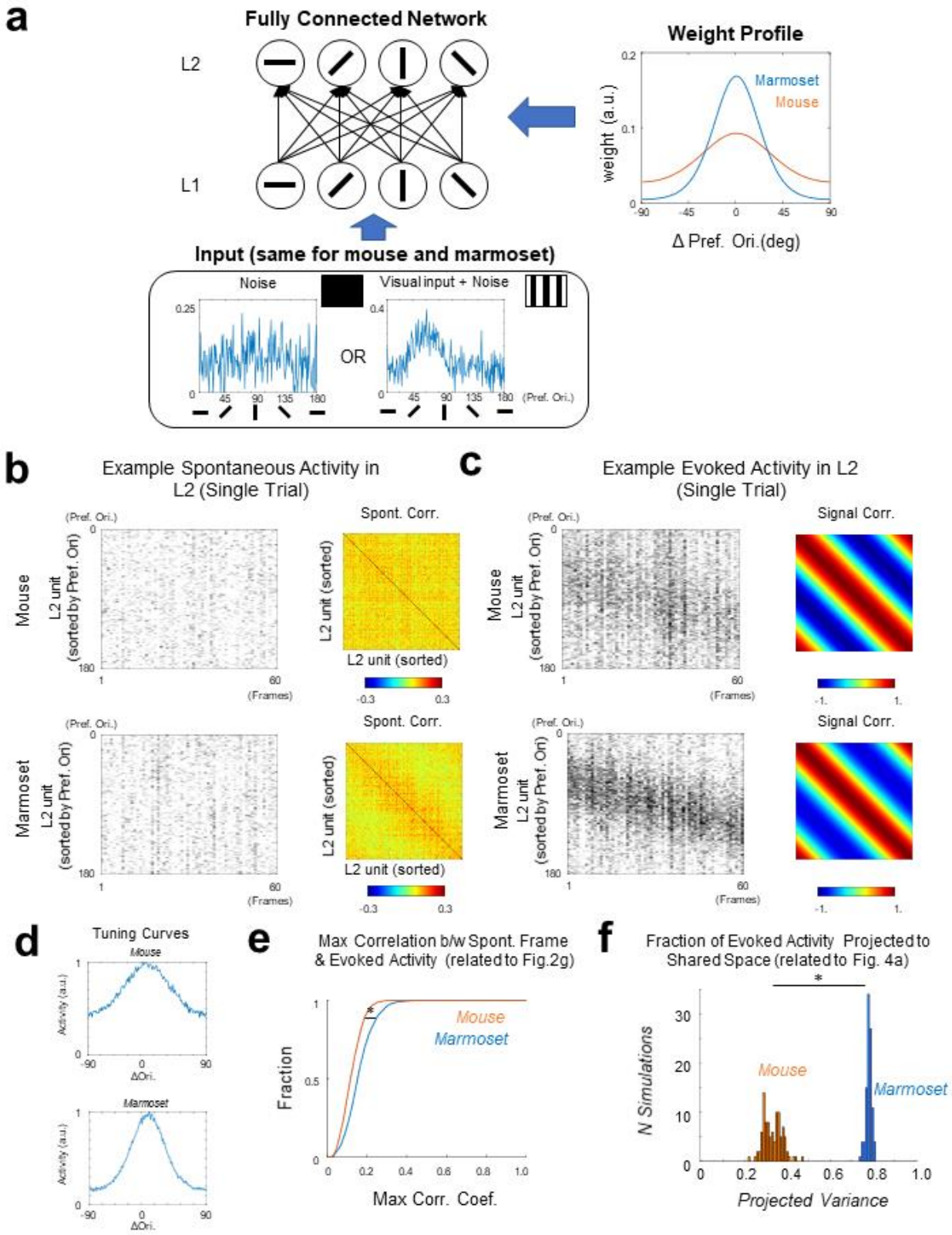
a
Fully Connected Network
L2
L1
Weight Profile
Marmoset
Mouse
weight (a.u.)
Δ Pref. Ori.(deg)
Input (same for mouse and marmoset)
Noise
Visual input + Noise
OR
(Pref. Ori.)
b
Example Spontaneous Activity in L2 (Single Trial)
Mouse
Marmoset
L2 unit (sorted by Pref. Ori)
(Frames)
Spont. Corr.
L2 unit (sorted)
c
Example Evoked Activity in L2 (Single Trial)
Signal Corr.
d
Tuning Curves
Mouse
Marmoset
Activity (a.u.)
ΔOri.
e
Max Correlation b/w Spont. Frame & Evoked Activity (related to Fig.2g)
Fraction
Max Corr. Coef.
f
Fraction of Evoked Activity Projected to Shared Space (related to Fig. 4a)
N Simulations
Projected Variance

Supplementary Figure 15 | A neural network simulation that tests the effect of structured versus examined functional architecture on the orthogonality between spontaneous and evoked activity. a) Model architectures. Two-layer fully connected networks with ReLU units are used. Preferred orientations are assigned to each unit. The inset in the bottom left shows examples of inputs to L1. In the simulation of spontaneous activities, L1 units receive structured noise inputs. In the simulation of visually evoked activities, L1 units receive orientation-dependent inputs plus structured noise inputs. Note that structured noise inputs are added to simulate single-trial activity. Connection weights between L1 and L2 units depend on the difference in the preferred orientation between units (inset in the right). The weight profile of marmoset V1 is made sharper than that of mouse V1 to resemble the structured organization in marmoset V1. Note that this difference in the weight profiles is the only difference between the mouse and marmoset V1 models. **b)** Example snapshots of spontaneous activity in L2 (right panels). Unit-wise correlations of spontaneous activity are also shown (left panels). **c)** Same as (b) but for visually evoked activities. **d)** Orientation tuning curves in example L2 units. **e)** Unit-wise correlation between spontaneous activities and trial-averaged visually evoked activities in L2. Same analysis and figure convention as in Fig. 2g. **f)** Fraction of stimulus-related variance projected to shared spaces. The same analysis as in Fig. 4a. Histogram of the fractions across 100 simulations is shown.

Supplementary Discussions

Supplementary Discussion 1

In the marmoset V1, spontaneous and visually evoked activity patterns were similar. Conversely, in the mouse V1, the two types of activity patterns were dissimilar. This species difference may be related to another species difference of V1: the difference in the synaptic integration by visual cortical neurons. It has been reported that synaptic integration by visual cortical neurons differ across columnar and non-columnar mammals: Synaptic inputs to a single neuron are more likely to share similar function in the columnar visual cortex than in the non-columnar visual cortex (*1-3*). Neurons sharing the same preferred orientation tend to have high noise correlation (*4, 5*) as well as spontaneous correlation (*6*). In the marmoset V1 in which orientation columns are present, local synaptic inputs to a single neuron are likely to share similar preferred orientations (*7, 8*). Hence, a marmoset V1 neuron tends to receive correlated spontaneous synaptic inputs. The correlated activity of presynaptic neurons activates the postsynaptic neuron sharing the same preferred orientation. Such a cascade of activity likely explains the correlated spontaneous activity of neurons sharing similar preferred orientations. In contrast, because of the absence of orientation columns, a mouse V1 neuron tends to receive local inputs from neurons whose preferred orientation are diverse. Thus, a mouse V1 neuron likely receives less correlated spontaneous synaptic inputs compared with a marmoset V1.

To test the validity of this hypothesis, we created simple two-layer neural network models that mimicked the marmoset or mouse V1 and examined whether a more disordered structure in mice leads to the orthogonalisation of spontaneous and stimulus-driven activity (**Supplementary Figure 15**) (see section "Details of Neural Network Simulations" below for details). A two-layer fully connected network was used as the base architecture for both the marmoset and the mouse V1 models. In this model, the visual inputs were orientation-selective neural activity (such as the neural activity in layer 4 of mouse V1) (L1 in **Supplementary Figure 15a**). The neurons in the input layer are connected to the top layer (L2) in an all-to-all fashion but with different weights. Ordered vs. disordered architectures (i.e. columnar vs. salt-and-pepper architectures) of the marmoset and mouse V1, respectively, are modeled by two distinct profiles of connection weights as functions of difference in preferred orientations of the connected neurons (right panels in **Supplementary Figure 15a**). The marmoset V1 model has a narrowly tuned weight profile with respect to the difference in preferred orientations of the connected neurons, so that a neuron in L2 preferentially samples inputs

from L1 neurons sharing similar preferred orientation. In contrast, the mouse V1 model has a broadly tuned weight profile, such that a neuron in L2 samples inputs from L1 neurons with diverse preferred orientations. The weight profile of the mouse V1 model was chosen based on previous physiological studies reporting that mouse L2/3 neurons receive broadly orientation-selective inputs (*4*). In this model, we assumed that neurons in the columnar cortical circuit (the marmoset V1) preferentially receive inputs from functionally similar neurons. Although similar bias toward inputs from functionally similar neurons exists in the salt-and-pepper type cortical circuit (i.e. the mouse V1)(*9*), the bias is likely much weaker than that in the columnar cortical circuit (*8*). It should be noted that columnar arrangements of neuronal cell bodies do not necessarily define connectivity among those neurons. Similarly, sharp integration of inputs is possible in the absence of orientation columns. To determine whether these possibilities are biologically plausible, detailed simulations of the developmental processes of the visual cortex would be necessary. Because such simulations are beyond the scope of this study, we modeled the effects of the presence and absence of orientation columns by sharp and broad integrations of inputs based on the empirical observations mentioned above (*8, 9*). We also note that there are other limitations in the biological plausibility of the model (*e.g.*, absence of inhibitory neurons, ReLU units), which could play an essential role in the real cortical circuit. The purpose of the model is only to demonstrate, in a simple setting, that differences in synaptic integrations could cause the difference in orthogonality between spontaneous and stimulus-evoked activities.

We ran simulations of visually evoked activity and spontaneous activity using these networks (bottom panels in **Supplementary Figure 15a**): For the simulation of spontaneous activity, we injected a structured noise into L1 neurons. The structured noise is modeled based on previous reports showing the similarity of signal correlation and noise correlation. In both primates and rodents, previous studies showed that V1 neurons with high signal correlation, hence similar preferred orientations, also showed high noise correlation and spontaneous activity correlation (*4, 10*). To simulate these previous observations, we convolved a white noise by using a Von Mises function to introduce noise correlation between L1 units sharing similar preferred orientations. **Supplementary Figure 15b** shows examples of simulated spontaneous activity in the mouse V1 and marmoset V1 models. Although the structured noise inputs to L1 neurons are the same for the marmoset V1 model and the mouse V1 model, correlated activities in L1 neurons are weighted more by each L2 neuron in the marmoset V1 model than the mouse V1 model because of a narrower

tuning of the weight profile in the marmoset V1 model. Thus, L2 neurons sharing similar preferred orientations in the marmoset V1 model should show correlated spontaneous activity. On the other hand, L2 neurons sharing similar preferred orientations in the mouse V1 model should show less correlated spontaneous activities, because each L2 neuron exerts more weights on diverse (less correlated) inputs from L1 neurons. Consistently, the activity correlation between L2 neurons revealed a more structured correlation matrix for the marmoset V1 model than for the mouse V1 model (right panels in the **Supplementary Figure 15b**). To simulate visually evoked activity, in addition to structured noise, we injected activity tuned at a selected preferred orientation into L1 neurons, mimicking the presentation of oriented gratings. **Supplementary Figure 15c** shows examples of simulated visually evoked activity in the mouse V1 and marmoset V1 models. Activity correlation between L2 neurons ("signal correlation") was similar for the two models (right panels in **Supplementary Figure 15c**). The orientation tuning curve of each L2 neuron was narrower in the marmoset V1 model than in the mouse V1 model, mimicking previous animal studies (*11, 12*). These correlation structures suggest that spontaneous activity patterns and visually evoked activity patterns were similar, at least in the correlation structure, in the marmoset V1 model but not in the mouse V1 model.

To confirm that the simulation reproduced essential patterns of the animal results, using the simulated data, we conducted the same analyses that we used for the animal data. As shown in Figure 2g, the maximum correlation value between the spontaneous and evoked-activity frames was significantly higher in the marmoset V1 model than in the mouse V1 model ($p < 10^{-42}$, rank-sum test; **Supplementary Figure 15e**). Similarly, as shown in Figure 4a, the fraction of the variance of visually evoked activity projected to the shared space was larger for the marmoset V1 model than for the mouse V1 model ($p < 10^{-33}$, rank-sum test across 100 instances of model pairs; **Supplementary Figure 15f**). These simulation results are consistent with animal data and suggest that spontaneous and visually evoked activity are more orthogonalized in the mouse V1 model than in the marmoset V1 model. Taken together, these results suggest that a more disordered connection leads to greater orthogonalization between spontaneous and evoked activities.

Details of Neural Network Simulations

Model architectures

Neural network simulations were conducted using Matlab (MathWorks, Natick, MA). The number of neurons in each model layer was set to 180. For each neuron, we assigned a unique preferred

orientation θ ranging from 1° to 180°.

The connection weight (W) between the θ-th neuron in layer 2, whose preferred orientation is θ deg, and a layer 1 neuron, whose preferred orientation is φ deg, was determined by a normalized Von Mises function as follows:

$$W'_x = \exp\left(A * \left(\cos\left(\frac{x * pi}{90}\right) - 1\right)\right) \quad (1)$$

$$W_{\theta-\varphi} = \frac{W'_{\theta-\varphi}}{\sum_i W'_i} \quad (2)$$

where A is a parameter of the Von Mises function, and an index i in the summation spans from 1 to 180 at a step equal to 1.

We separately set the connection weight W for the marmoset ($W_{marmoset}$) and the mouse (W_{mouse}) models, such that the mouse layer 2 neurons receive broader orientation-selective inputs than the marmoset model; A = 1.8 for $W_{marmoset}$; A = 0.6 for W_{mouse} (see Supplementary Fig. 15a).

Generation of visually-evoked and spontaneous activities

For the generation of spontaneous activity, we first generated random noise activities independently sampled from a normal distribution:

$$\mathbf{n}_0 = \{n_{0\_1}, n_{0\_2}, \ldots, n_{0\_\theta}\},\ n_{0\_\theta} \sim \mathcal{N}(0,1) \quad (3)$$

These activities were rectified by a threshold value t_0 (t_0 = 0.1):

$$\mathbf{r}_0 = \mathrm{relu}(\mathbf{n}_0, t_0) \quad (4)$$

Then, these activities were convolved with a weight kernel w:

$$w'_x = \exp\left(\cos\left(\frac{x * pi}{90}\right) - 1\right) \quad (5)$$

$$w_x = \frac{w'_x}{\sum_i w'_i} * 0.5 \quad (6)$$

$$r_{0\_\theta} = \sum_{k=\theta-90}^{\theta+89} w_{\mathrm{mod}(k,180)} * r_{0\_k} \quad (7)$$

where an index i runs from 1 to 180 at a step equal to 1.

Finally, a random noise was added to each of the activities with an arbitrary coefficient to obtain

input to layer 1 neurons ($\mathbf{r}_{\text{sponta}}$):

$$\mathbf{n_1} = \{n_{1_1}, n_{1_2}, \dots, n_{1_\theta}\},\ n_{1_\theta} \sim \mathcal{N}(0,1) \quad (8)$$

$$\mathbf{r}_{\text{sponta}} = \mathbf{r}_0 + \mathbf{0.05} * \mathbf{n}_1 \quad (9)$$

For the generation of visually-evoked activity, we first generated a spontaneous input to L1 neurons ($\mathbf{r}_{\text{sponta}}$), created as described above, and then generated a visual input $\mathbf{V} = \{V_1, V_2, \dots, V_{180}\}$ as explained below.

Visual input with the stimulus orientation ϑ deg to the θ-th neuron in layer 2, whose preferred orientation is θ deg, was defined by the Von Mises function:

$$V'_{\theta,\vartheta} = \exp\left(2.5 * \left(\cos\left(\frac{(\theta - \vartheta) * \text{pi}}{90}\right) - 1\right)\right) \quad (10)$$

$$V_{\theta,\vartheta} = \frac{V'_{\theta,\vartheta}}{\sum_k V_{k,\vartheta}} \quad (11)$$

where an index k runs from 1 to 180 at a step equal to 1. The stimulus orientations (ϑ) spanned from 1 deg to 180 deg at a 1 deg step (i.e. $\vartheta \in \{1,2,\dots,180\}$).

Then, a visual input of L1 neurons ($\mathbf{r_{vis}}$) was obtained using the following equation:

$$\mathbf{r_{vis}} = \mathbf{r}_{\text{sponta}} + 9.0 * \mathbf{V} \quad (12)$$

Activities of layer 1 neurons ($\mathbf{R}_1$) were obtained by rectifying inputs to L1 neurons by a threshold value t_1 ($t_1 = 0.1$):

$$\mathbf{R}_1 = \text{relu}(\mathbf{r}_{\text{input}}, t_1) \quad (13)$$

where $\mathbf{r}_{\text{input}}$ is $\mathbf{r_{sponta}}$ and $\mathbf{r_{vis}}$ for spontaneous and visually evoked activities, respectively.

An input from layer 1 neurons to the θ-th neuron in layer 2, whose preferred orientation is θ deg, can be expressed as:

$$r2_\theta = \sum_{k=\theta-90}^{\theta+89} W_k * R1_k \quad (14)$$

where the $\mathbf{R1} = \{R1_1, R1_2, \dots, R1_{180}\}$ and the $\mathbf{r2} = \{r2_1, r2_2, \dots, r2_{180}\}$ correspond to the activity (output) of layers 1 neurons and inputs to 2 neurons, respectively.

Next, a random noise was further added to the layer 2 neuron input with:

$$\mathbf{r2}_{\text{noisy}} = \mathbf{r2} + 0.05 * \mathbf{n}_2 \quad (15)$$

$$\mathbf{n}_2 = \{n_{2\_1}, n_{2\_2}, \dots, n_{2\_\theta}\},\ n_{2\_\theta} \sim \mathcal{N}(0,1) \quad (16)$$

Finally, the layer 2 neuron activity was rectified by a threshold value t_2 ($t_2 = 0.1$):

$$\mathbf{R2} = \mathrm{relu}\left(\mathbf{r2}_{\mathrm{noisy}}, \mathrm{t}_2\right) \quad (17)$$

For visually evoked activity, a total of 1000 visual stimulation runs, yielding 180,000 activity patterns (which we call frames) were generated. For spontaneous activity, a total of 1000 frames of spontaneous activity simulation were generated. In both visual stimulation runs and spontaneous activity runs, individual frames were treated as independent. A code used for the simulation is available for download (https://github.com/teppei-matsui/NN_Simulation).

Orientation tuning width for each L2 unit was obtained by fitting the Von Mises function to trial averaged orientation responses, with A, W and θ as free parameters:

$$VM(x, A, W, \theta) = \mathrm{A} * \exp\left(W\left(cos\left(\frac{(\mathrm{x} - \theta) * \mathrm{pi}}{90}\right) - 1\right)\right)$$

Analysis of simulated spontaneous and visually evoked activities was conducted similarly as for mouse and marmoset data. In the calculation of the fraction of visual stimulus-related variance projected to the shared space (Supplementary Fig. 15f), we used 20 spontaneous PCs to obtain shared space. A total of 100 instances of simulations were conducted to generate the distribution of the fraction of projected variances.

Supplementary Discussion 2

The progressive orthogonalization of spontaneous and stimulus-evoked activity patterns may be explained by the concept of communication subspace of cortico-cortical connections (*13, 14*). In the macaque visual cortex, V1 activity patterns contained in the communication subspace are more likely to evoke downstream activity in V2 (*13*). We conjecture that the activity patterns of stim-only PCs are more effective in activating neurons in the downstream area, thus constituting the communication subspace. In contrast, the activity patterns of shared PCs are less effective in activating down-stream neurons. After multiple steps of cortico-cortical activity propagations, activity patterns corresponding to shared PCs are diminished whereas the patterns corresponding to stim-only PCs are efficiently propagated.

References for Supplementary Discussion

1. L. Cossell *et al.*, Functional organization of excitatory synaptic strength in primary visual cortex. *Nature* **518**, 399–403 (2015).
2. D. Wilson *et al.*, Orientation selectivity and the functional clustering of synaptic inputs in primary visual cortex. *Nat Neurosci* **19,** 1003–1009 (2016).
3. M. F. Iacaruso, I. T. Gasler & S. B. Hofer, Synaptic organization of visual space in primary visual cortex. *Nature* **547**, 449–452 (2017).
4. H. Ko *et al.*, Functional specificity of local synaptic connections in neocortical networks. *Nature* **473**, 87-91 (2011).
5. G. C. DeAngelis, G. M. Ghose, I. Ohzawa, R. D. Freeman, Functional micro-organization of primary visual cortex: receptive field analysis of nearby neurons. *J Neurosci* **19**, 4046-4064 (1999).
6. I. Nauhaus, L. Busse, M. Carandini, D. L. Ringach, Stimulus contrast modulates functional connectivity in visual cortex. *Nat Neurosci* **12**, 70-76 (2009).
7. B. Scholl, D. E. Wilson, D. Fitzpatrick, Local Order within Global Disorder: Synaptic Architecture of Visual Space. *Neuron* **96**, 1127-1138.e1124 (2017).
8. D. E. Wilson, D. E. Whitney, B. Scholl, D. Fitzpatrick, Orientation selectivity and the functional clustering of synaptic inputs in primary visual cortex. *Nat Neurosci* **19**, 1003-1009 (2016).
9. T. W. Chen *et al.*, Ultrasensitive fluorescent proteins for imaging neuronal activity. *Nature* **499**, 295-300 (2013).
10. A. Kohn, M. A. Smith, Stimulus dependence of neuronal correlation in primary visual cortex of the macaque. *J Neurosci* **25**, 3661-3673 (2005).
11. C. M. Niell, M. P. Stryker, Highly selective receptive fields in mouse visual cortex. *J Neurosci* **28**, 7520-7536 (2008).
12. H. H. Yu, M. G. Rosa, Uniformity and diversity of response properties of neurons in the primary visual cortex: selectivity for orientation, direction of motion, and stimulus size from center to far periphery. *Vis Neurosci* **31**, 85-98 (2014).
13. J. D. Semedo, A. Zandvakili, C. K. Machens, B. M. Yu, A. Kohn, Cortical Areas Interact through a Communication Subspace. *Neuron* **102**, 249-259.e244 (2019).
14. A. Kohn *et al.*, Principles of Corticocortical Communication: Proposed Schemes and Design Considerations. *Trends Neurosci* **43**, 725-737 (2020).